Solvent Isotope Effect on Biomolecular Adsorption at Hydrophobic Surfaces

Tasha A. Jarisz, Kailash C. Jena, Matthew C. Dixon, and Dennis K. Hore

July 2017

The final publication is available at ACS Publications via:
https://doi.org/10.1021/acs.jpcc.7b05377

# Solvent Isotope Effect on Biomolecular Adsorption at Hydrophobic Surfaces

Tasha A. Jarisz,[†] Kailash C. Jena,[†] Matthew C. Dixon,[‡] and Dennis K. Hore[*,†]

†*Department of Chemistry, University of Victoria, Victoria, British Columbia, V8W 3V6, Canada*

‡*Biolin Scientific Inc., 215 College Road, Suite 300, Paramus NJ 07652*

E-mail: dkhore@uvic.ca

## Abstract

In vibrational studies of biological systems, $D_2O$ is often substituted for $H_2O$ in order to more clearly resolve the amide I and C–H stretching regions. However, in interfacial studies where adsorption is involved, the difference between these two solvents may play a role in the amount adsorbed and, consequently, the adsorbed structure. Nonlinear vibrational spectroscopy reveals striking differences in the spectral signature of the hydrophobic amino acid leucine adsorbed on polystyrene in the presence of light vs heavy water. Dissipation-monitoring quartz crystal microbalance studies conclude that more amino acid is present on the hydrophobic surface when the solvent is $D_2O$, and the relative surface populations account for the difference in spectral intensity. This finding has consequence for surface structural studies, and provides insight into the role of solvent in biomolecular adsorption at hydrophobic surfaces.

# Introduction

An understanding of the interaction of molecules in solution with hydrophobic surfaces is of fundamental importance to the enhanced biocompatibility of materials used for medical implants,[1–3] bio-separation and purification technologies,[4–9] and the development of biosensors.[10–12] The adsorption of proteins onto polymers is a multi-faceted phenomenon that is governed by the chemical composition and solution structure of the protein, the nature of the polymer substrate, temperature, pH, and the presence of other solutes. One of the challenges associated with characterizing adsorption at solid–liquid interfaces is achieving sufficient specificity for the surface in the presence of the adjacent bulk substrate and solution phases. In recent years, visible-infrared sum-frequency generation (SFG) spectroscopy has emerged as a premier technique for studying the structure of adsorbed molecules.[13–15] It is particularly attractive for probing the interface between two centrosymmetric media, such as the solution–isotropic solid interface.[16–18] This is because, under the electric dipole approximation, the second-order nonlinear susceptibility, $\chi^{(2)}$, equals zero in the bulk phases, but is non-zero at the interface where the symmetry is broken. In the case of molecules at interfaces, the requirement that $\chi^{(2)} \neq 0$ necessitates that they be oriented in a polar manner. As a consequence, molecules can be situated very near the interface but, if they are not adsorbed, they will not be oriented and therefore remain undetected by SFG. In contrast to evanescent-wave techniques such as ATR-IR, or bulk spectroscopic probes that require grazing angles to achieve surface-specificity, SFG spectroscopy provides an exquisite sensitivity to the interface since it is the symmetry of the molecular environment that governs its response. These measurements, together with associated modeling techniques, provide a feature-rich description of the structure of molecules adsorbed on surfaces.[19–21]

There has been considerable development in the quantitative analysis of SFG spectra to reveal the orientation and orientational distribution of interfacial molecules.[22] However, it is often challenging to separate effects arising from the number of molecules at the interface from those due to the arrangement of the molecules. For example, decreasing the number of molecules, or reducing their polar order parameter will both result in a decrease in $\chi^{(2)}$ and therefore a reduction in SFG

intensity. Thus, a complementary technique is needed to attribute changes in signal intensity to either alignment or population differences. The quartz crystal microbalance with dissipation monitoring (QCM-D) is a high-resolution mass-sensing technique. A QCM sensor oscillates at a specific frequency when a voltage is applied, which is directly related to the mass of adsorbed molecules, according to the Sauerbrey relation.[23] For rigid films in a vacuum, the Sauerbrey equation is sufficient to relate such changes in frequency to the mass of the adsorbed layer; However, it fails for soft, viscoelastic films or under liquid conditions. In these cases, another model, such as the Voigt model, must be used. In addition to measuring frequency changes, QCM-D instruments can also measure dissipation, or energy loss in the film, which is related to the viscosity and elasticity of the molecular layer.[23] By measuring both the frequency and dissipation shifts for several harmonics, the Voigt model can be applied in order to obtain the absorbed mass and viscoelastic properties of the film.[24] Within the last decade, QCM-D has become integral to studying molecular systems at solid-liquid interfaces, including the adhesion of complex polymer and biochemical systems.[25,26] In recent years, its capabilities have been combined with optical techniques such as ellipsometry,[27,28] IR absorption,[29,30] and SFG spectroscopy.[31–35]

Substitution of $D_2O$ for $H_2O$ as a solvent is commonly used for investigations of biological systems by magnetic resonance because of their nuclear spin differences,[36] and by IR absorbance and other vibrational techniques in order to eliminate interferences in the C–H stretching region. In protein studies, $D_2O$ is preferentially used as a solvent so that the backbone amide I stretching modes of the protein can be studied without interference from $H_2O$ bending modes.[37] The greater strength of the O-D–O bond in $D_2O$ than the corresponding hydrogen bond in water[38] results in greater structural ordering of $D_2O$..[36] This is significant as the formation and disruption of both intra- and intermolecular hydrogen bonds governs protein dynamics, which in turn dictates the structure of proteins in solution. A stronger hydrogen bond would increase solvent-solvent interactions, but would decrease the ability of the solvent to interact with hydrophilic regions on the protein. Proteins in $D_2O$ also adopt a compressed, less flexible structure and therefore have a greater entropy and enthalpy of unfolding.[36,39] This can be attributed to the less effective

solvation of hydrophobic groups at the protein surface, resulting in reduced solvent exposure of these hydrophobic regions.[38] Many studies have demonstrated that even small changes in the nature of the solvent, such as an H to D substitution, have significant effects on the stability and thermodynamic behaviour of proteins.[38–40] As a result, it is critical to understand not only the consequences of such a substitution on peptide and protein solvation and stability, but also its effects on their adsorption capabilities and structure at interfaces. The combination of hydrophobic surface and hydrophobic side chain was chosen here due to the greater perturbation of interfacial water structure at hydrophobic surfaces.[41,42] Moreover, for such a system, the major driving force for adsorption is the hydrophobic interactions between them, while electrostatic interactions with the surface become negligible. By investigating adsorption of an amino acid, the effects of isotopic solvent substitution are expected to be more pronounced since small, zwitterionic species adsorb to hydrophobic surfaces to a lesser extent than large, soft proteins. Leucine is an ideal choice for this study as it is small, has a hydrophobic side chain, is zwitterionic, and there are numerous experimental[21,33,43–48] and modelling[20,49–52] studies involving leucine adsorption to hydrophobic surfaces, either as an indiviual amino acid, or a component of a short synthetic peptide. We use a combination of QCM-D and vibrational SFG measurements to study leucine adsorption onto polystyrene surfaces from solutions of $H_2O$ and $D_2O$. We will illustrate that the ratio of adsorbed masses from the two solvents, obtained through Voigt modeling of the frequency and dissipation shift data, accounts for the marked difference in SFG spectra recorded for leucine at polystyrene–water and polystyrene–$D_2O$ interfaces.

# Methods

**Quartz crystal microbalance with dissipation monitoring.** The quartz crystal microbalance (QCM) measures changes in an oscillating quartz crystal resonant frequency when an AC voltage is applied (Fig. 1a). For rigid films, the Sauerbrey relation may be used to directly relate frequency changes to the mass of the adsorbed layer. However, for viscoelastic deposition in liquids, i.e the

adhesion of soft films, the resonant frequency of the crystal is altered by acoustic-fluid damping of the viscoelastic medium.[53] As a result, the shear wave decays very rapidly and the QCM probes only objects that are within a micron of the crystal surface, making it a surface-sensitive technique. Due to energy losses from the shear wave when travelling through less rigid adsorbed films, large changes in dissipation and resonant resistance also arise. Combining frequency shift measurements with changes in the dissipation factor have been termed QCM with dissipation (QCM-D). As a result, in addition to detecting mass changes, QCM-D sensors provide information about interactions with soft matter, in which changes in the density and viscoelastic properties of the film can be determined. When using QCM-D under liquid conditions, the density and viscosity of the solution, together with the softness of the adsorbed film, cause significant energy losses that must be taken into account.

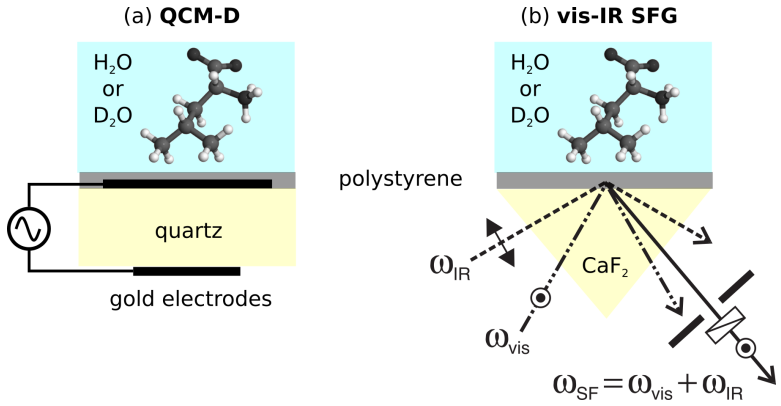


Figure 1: (a) QCM-D experiment with polystyrene-coated sensor surfaces next to leucine solutions. (b) SFG experimental geometry illustrating a p-polarized IR beam and s-polarized visible beam approaching an aqueous solution from within a polymer film. In the illustrated configuration, the s-component of the reflected SFG beam is detected, and recorded as a function of the incident IR energy.

In a damped environment, the Sauerbrey equation underestimates the adsorbed mass from the measured frequency shift.[54] As a result, the frequency changes alone are rarely able to characterize the entire system. With access to both the frequency shift $\Delta f_n$ and the dissipation shift $\Delta D_n$ for multiple harmonics $n$ in a QCM-D experiment, models such as Kevin-Voigt may be applied to characterize the viscoelastic parameters and provide a more accurate adsorbed mass.[23,24,55] When the viscoelastic layer is thin and the oscillator is immersed in the leucine solution, the frequency

and dissipation shifts are approximately given by

$$\Delta f_n^{\text{soln}} \approx -\frac{1}{2\pi\rho_0 h_0}\left[\frac{\eta_2}{\delta_2} + h_1\rho_1 n\omega_0 - 2h_1\left(\frac{\eta_2}{\delta_2}\right)^2 \frac{\eta_1 n^2\omega_0^2}{\mu_1^2 + (n\omega_0\eta_1)^2}\right] \tag{1a}$$

$$\Delta D_n^{\text{soln}} \approx \frac{1}{\pi n f_0\rho_0 h_0}\left[\frac{\eta_2}{\delta_2} + 2h_1\left(\frac{\eta_2}{\delta_2}\right)^2 \frac{\mu_1 n\omega_0}{\mu_1^2 + (n\omega_0\eta_1)^2}\right] \tag{1b}$$

where the acoustic wave penetration depth is

$$\delta_2 = \sqrt{\frac{2\eta_2}{\rho_2 n\omega_0}}. \tag{2}$$

In the above equations, $f_0 \approx 5$ MHz is the fundamental vibration frequency of the crystal, $\omega_0 = 2\pi f_0$, and $n$ is the harmonic number. $\rho_0 = 2148$ kg/m$^3$ is the density of the quartz crystal, $\rho_1$ is the density of the adsorbed layer, and $\rho_2$ is the density of the leucine solution. The viscosities of the layer and solvent are given by $\eta_1$ and $\eta_2$, respectively. The adsorbed layer of thickness $h_1$ has a shear elastic modulus $\mu_1$.

In typical QCM-D experiments, the frequency and dissipation changes resulting from adsorption of a solute in dilute solution are compared to the values measured in the absense of the solute (pure solvent or buffer). In such cases, Eq. 1 is simplified in practice since the shifts can be measured with respect to the solvent baseline, and all subsequent changes in $\Delta f$ and $\Delta D$ may be attributed to adsorption. In other words, in the limit of infinite dilution, the bulk solute and reference solvent have the same effect on the sensor surface. In our experiment, however, we are dealing with concentrated solutions and so the analysis is not as straightfoward since the reference solvent and bulk solution do not result in the same measured shifts prior to adsorption. We therefore perform an initial measurement with either pure water or pure $D_2O$, where the frequency and dissipation

factor shifts (with respect to air) are given by

$$\Delta f_n^{\text{solvent}} \approx -\frac{1}{2\pi\rho_0 h_0}\frac{\eta_2}{\delta_2} \tag{3a}$$

$$\Delta D_n^{\text{solvent}} \approx \frac{1}{\pi n f_0 \rho_0 h_0}\frac{\eta_2}{\delta_2}. \tag{3b}$$

The subscript 2 now refers to the water or $D_2O$ in the absence of any leucine. Our reported data, and subsequent modelling of the viscoelastic properties of the adsorbed layer, is then represented by

$$\Delta f_n = \Delta f_n^{\text{soln}} - \Delta f_n^{\text{solvent}} \tag{4a}$$

$$\Delta D_n = \Delta D_n^{\text{soln}} - \Delta D_n^{\text{solvent}}. \tag{4b}$$

**Nonlinear vibrational spectroscopy.** In visible-infrared sum-frequency generation (SFG) experiments, a high intensity visible and infrared laser are spatially- and temporally-overlapped at the interface of interest (Fig. 1b). In the electric dipole approximation, molecules in non-centrosymmetric environments (substrate surface, adsorbates, and aligned interfacial water) contribute to $\chi^{(2)}$ and one measures

$$I_{\text{SFG}} \propto \frac{\omega_{\text{SFG}}^2}{n_{\text{SFG}} n_{\text{vis}} n_{\text{IR}} \cos^2\theta_{\text{SFG}}} \left|(L_{yy}e_y)_{\text{SFG}}\chi^{(2)}_{yyz}(L_{yy}e_y)_{\text{vis}}(L_{zz}e_z)_{\text{IR}}\right|^2 I_{\text{vis}} I_{\text{IR}} \tag{5}$$

where $I_i$ are the intensities of the detected SFG beam, and the input visible and IR pump beams, $\omega_{\text{SFG}} = \omega_{\text{vis}} + \omega_{\text{IR}}$, $n_i$ are the refractive indices of the incident medium, and $\theta_{\text{SFG}}$ is the angle of the reflected SFG beam. In our experiment, we apply s-polarized visible and p-polarized infrared beams, and detect the s-polarized component of the SFG. As shown in Eq. 5, this is a measure of $\chi^{(2)}_{yyz}$. In this work, it is particularly important to consider not the incident but the surface fields

obtained from

$$L_{yy,\mathrm{SFG}} = 1 + r_{s,\mathrm{SFG}} \tag{6a}$$

$$L_{yy,\mathrm{vis}} = 1 + r_{s,\mathrm{vis}} \tag{6b}$$

$$L_{zz,\mathrm{IR}} = 1 + r_{p,\mathrm{IR}} \tag{6c}$$

where $r_s$ and $r_p$ are the conventional s- and p-polarized Fresnel reflection coefficients, and the unit polarization vectors $e_{y,\mathrm{SFG}} = e_{y,\mathrm{vis}} = 1$, $e_{z,\mathrm{IR}} = \sin\theta_{\mathrm{IR}}$. As $r_s$ and $r_p$ are functions of the refractive index, their dispersion must be taken into account. Literature refractive index data for polystryene,[56] $CaF_2$,[57] $H_2O$,[58] and $D_2O$[59] were used for this calculation. The real and imaginary components of the water and $D_2O$ refractive index are plotted in Fig. 2a and b. As Eq. 5 indicates, the relevant correction involves the square of the product of the local field factors, as plotted in Fig. 2c. The spectra we present are corrected for these factors, which can vary considerably between the two solvents according to the wavelengths, polarization of the fields, and beam angles. Our results are therefore proportional to $|\chi^{(2)}(\omega_{\mathrm{IR}})|^2$, as the other factors that depend on $\omega_{\mathrm{IR}}$ have been removed and we are directly comparing the water and $D_2O$ $|\chi^{(2)}_{yyz}|^2$ spectra. These factors are highly sensitive to the polarization of the beams, and the angle of the incident fields. For our experimental geometry, Fig. 2 illustrates that the relative correction is in the range 0.5–1.5, and has a significant frequency dependence.

**Sample preparation and measurements.** QCM-D experiments were performed with temperature-controlled sensor chambers (Q-Sense, Gothenburg, Sweden) and a peristaltic pump, in order to maintain a constant temperature of 23 ± 0.02°C and 0.1 mL/min flow rate. Polystyrene-coated quartz crystal sensors of 0.3 mm thickness and 14 mm diameter were initially cleaned by rinsing and soaking with water, rinsing with ethanol, and then dried under nitrogen. The pure solvents ($H_2O$ and $D_2O$) were pumped through until each liquid filled the chamber, and then resonant frequencies of the fundamental and harmonics were measured in the presence of the solvent. Once a baseline was established after approximately 30 min, an unbuffered 0.17 M solution of L-leucine (Sigma

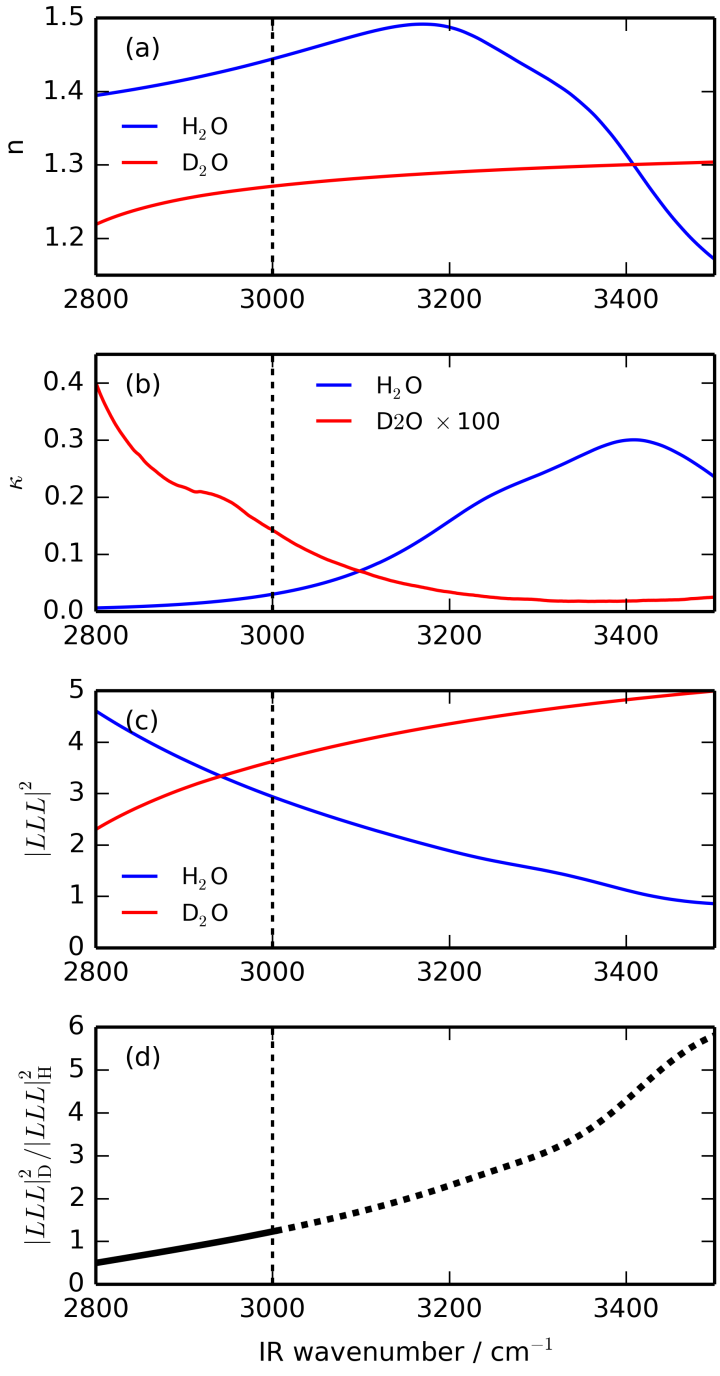


Figure 2: (a) Real part of the water (blue) and $D_2O$ (red) refractive index, (b) imaginary part of the refractive indices, (c) corresponding local field correction to the SFG intensity, (d) ratio of the $D_2O/H_2O$ corrections.

Aldrich, Oakville, ON) in 18.2 MΩ·cm $H_2O$ or $D_2O$ (Sigma Aldrich) was flowed through the chamber. Frequency and dissipation versus time curves were collected. After $\Delta f_n$ and $\Delta D_n$ reached a stationary state, pure solvent was used as a rinse to remove any leucine adhered reversibly to the sensor surface. The sensor chamber and pump tubes were cleaned between replicate experiments by pumping a 2% Hellmanex solution (Sigma-Aldrich Z805939) for 15 min, followed by 18.2 MΩ·cm $H_2O$ for 15 min.

Surfaces for SFG spectroscopy were prepared by spin-coating a 2% w/w solution of polystyrene-$d_8$ in deuterated toluene onto $CaF_2$ dove prisms (Del Mar Photonics, CA) at 2000 rpm, and then annealing at 100°C for 1 h. The deuterated polymer enables leucine methylene vibrations to be observed. Although protonated polystyrene was used in the QCM-D study, previous accounts of organic molecules on polystyrene surfaces have found the adsorbed structure to be the same regardless of whether the polystyrene substrate was deuterated or protonated.[60,61] Leucine was dissolved in either 18.2 MΩ·cm water or $D_2O$ (Sigma Aldrich) to achieve a concentration of 0.17 M, and introduced into a custom teflon sample cell.[18] This was the mininum concentration at which C-H stretching modes could be observed clearly in water. Details of the experimental configuration have been described previously.[18] In brief, a 25 ps Nd:YAG laser (Ekpla PL2241A) was used to create the 532 nm visible pump beam, and 2800–3600 $cm^{-1}$ tuneable IR pump beam through parametric generation (Ekspla PG501). The visible beam was incident onto the polystyrene-coated $CaF_2$ prism at 70° with a beam size of 1 mm and a pulse energy of 110 $\mu$J. The infrared beam was incident at 75°, focused to 0.5 mm diameter, 200 $\mu$J/pulse. Spectra were collected by measuring the SFG intensity with a gated PMT (Hamamatsu R7899) at each IR frequency in steps of 2 $cm^{-1}$ in the 2800–3000 $cm^{-1}$ range, and 5 $cm^{-1}$ in the 3000–3600 $cm^{-1}$ region, averaging 100 pulses at each IR step.

# Results and Discussion

## QCM-D

**Fitting the QCM-D data.** Fig. 3 illustrates the frequency ($\Delta f_n/n$) and dissipation ($\Delta D_n$) shifts after pure $D_2O$ and $H_2O$ were replaced with heavy and light leucine-water solutions. (Note that we are following the convention that this normalization to the harmonic number $n$ is explicit for $\Delta f$, but implicit for $\Delta D$ based on the expressions as they appear in Eq. 1.) Data for the fundamental ($n = 1$) are not used as a result of mounting stress effects, as is typical for QCM experiments. The penetration depth of the acoustic wave at each frequency varies as a result of the bulk density and viscosity changes going from $H_2O$ and $D_2O$ to leucine solutions, as well as any adsorbed, solvent-associated leucine molecules that couple to the polystyrene surface and dampen the oscillation. Lower harmonics have a greater penetration depth than higher harmonics, as indicated by Eq. 2. We should clarify that the time dependence of these signals, of central interest to most QCM-D studies, has no significance for us. This is because the adsorption is faster than the mixing time in the pump chamber. Any apparent changes in $\Delta f$ and $\Delta D$ with time are largely due to the difference in bulk liquid properties as the pure solvent is replaced with solution inside the chamber. Using code developed in-house, data for the six harmonics were fit to Eq. 4 to extract the adsorbed layer thickness $h_1$, shear viscosity $\eta_1$, and shear elastic modulus $\mu_1$. To account for changes in the bulk liquid properties as a result of the relatively high concentration of the leucine solution, the bulk viscosity of the leucine-$H_2O$ and leucine-$D_2O$ solutions were also fit using our measured bulk solution densities of $\rho_2$ = 999.2 kg/m$^3$ and 1108 kg/m$^3$ respectively. These values were obtained by weighing solutions of known concentration prepared in volumetric flasks.

The difference between the calculated (solid circles in Fig. 3) and experimental values (open circles in Fig. 3) was minimized using a truncated Newton's method.[62] Resulting parameters are shown in Table 1. One notices that the layer viscosities, in both $H_2O$ and $D_2O$, are similar to that of the bulk solutions, indicating that the adsorbed layer is liquid-like. The loss tangent $\omega\eta/\mu$ was calculated to be $\approx$ 1.5 for $H_2O$ and $\approx$ 2 for $D_2O$, at the fundamental frequency $\omega$. These values are

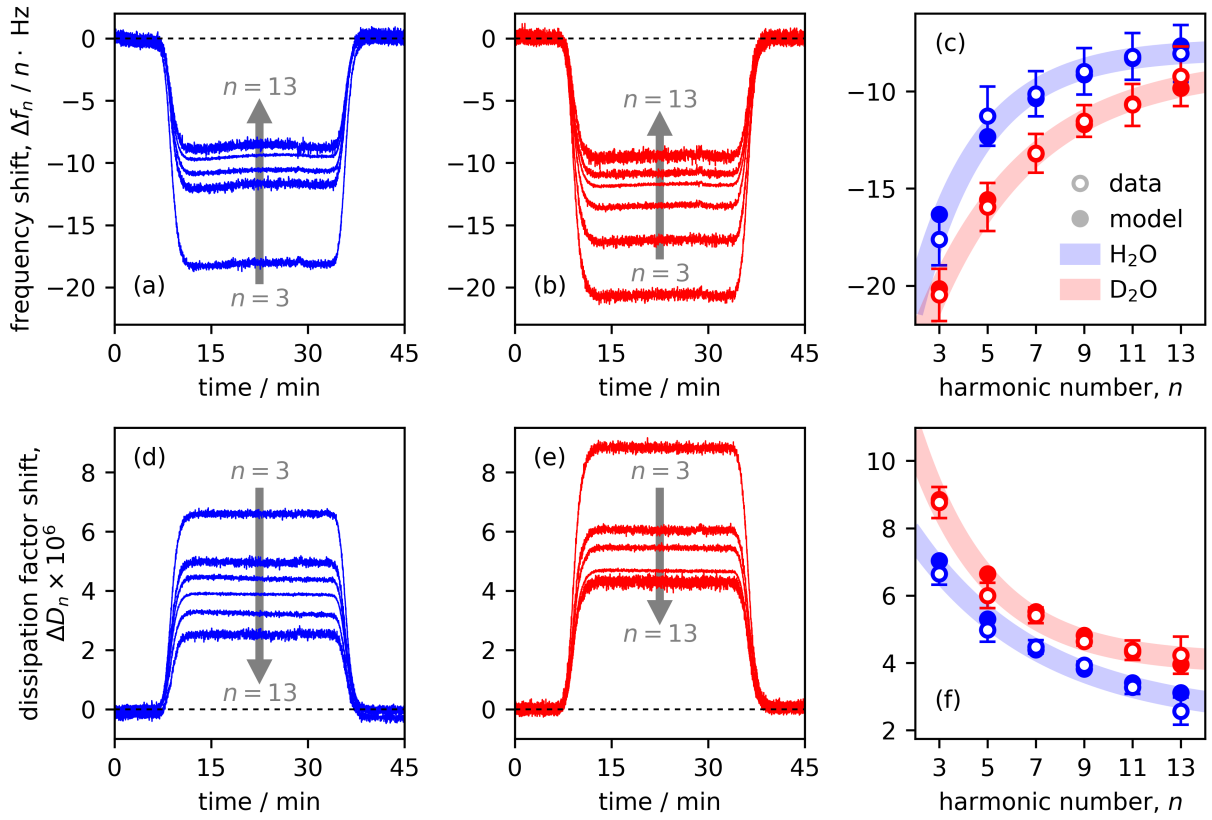


Figure 3: (a)-(c) Measured equilibrium frequency shifts, normalized to the harmonic $n$, on polystyrene-coated quartz sensors when the environment is changed from $H_2O$ to a 0.17 M solution of leucine in $H_2O$ (blue traces and open circles in (c)), and from $D_2O$ to a 0.17 M solution of leucine in $D_2O$ (red traces and open circles in (c)). (d)-(f) Simultaneously measured shift in dissipation factor. In all cases, filled circles are the result of fitting to the model in Eq. 4. Error bars indicate one standard deviation.

in the range of what has been reported for adsorption of other species from aqueous solutions,[63,64] including the similarity between the values in the two solvents.[63]

**Implication for surface coverage.** The values returned by the fitting also enable us to calculate the adsorbed mass of the leucine layer in $H_2O$ as 153 ± 28 ng/cm$^2$, and 339 ± 58 ng/cm$^2$ in $D_2O$. We can provide some further insight into these values by considering how they translate into surface coverage. It has been shown that leucine prefers to adopt a standing conformation at the polystyrene-water interface, rather than one lying flat on the surface.[21] This is because a standing conformation minimizes interactions between the hydrophobic alkyl groups and the hydrophilic, charged amino and ester moieties. Moreover, the alkyl groups are able to occupy regions of lower

solvent density nearer the surface, while allowing the zwitterionic portion of the amino acid to be more solvated by the bulk solution. This effect would be enhanced in $D_2O$ since there would be a greater energetic penalty for disrupting the O–D bonding network; thus, the leucine molecules would be more inclined to orient in a standing conformation near the surface, leading to greater adsorption at the interface. Taking this proposed geometry into account from the structures in the simulations,[21] we assume an elliptical footprint with major axis ≈ 4 Å and minor axis ≈ 2 Å, resulting in an area of ≈ 6.3 Å$^2$. The adsorbed masses therefore correspond to 98% and 44% surface coverage for leucine in $D_2O$ and $H_2O$, respectively. In light of the above, the formation of a near monolayer in the case of $D_2O$ seems reasonable based on its increased preference for a standing orientation, resulting in a greater packing of the leucine molecules at the surface. In $H_2O$, where less adsorption occurs, since the leucine molecules still prefer a standing conformation at the hydrophobic surface, less than monolayer coverage is achieved.

**Difference in adsorbed mass.** Since the structure of the solvent plays a crucial role in the adsorption of amino acids, it is important to consider the effects of the water/$D_2O$ solvation environment on leucine adsorption. For a nonpolar amino acid like leucine adsorbing to a hydrophobic surface, the major driving force is the hydrophobic interactions between the side chain (in particular, the terminal methyl groups) and the substrate. It has been shown that the attractive potential exhibited by hydrophobic surfaces is too weak to hold solvent molecules close

**Table 1: Parameters used to fit the QCM-D data appearing in Fig. 3 to Eq. 4.**

| Property | Symbol | $H_2O$ value | $D_2O$ value | Units | Source |
|---|---|---|---|---|---|
| quartz frequency | $f_0$ | $4.958 \times 10^6$ | $4.952 \times 10^6$ | $s^{-1}$ | measured |
| quartz thickness | $h_0$ | $302.5 \times 10^{-6}$ | $302.9 \times 10^{-6}$ | m | derived |
| quartz density | $\rho_0$ | 2648 | 2648 | $kg{\cdot}m^{-3}$ | literature |
| solvent density | $\rho_2$ | 997.5 | 1107 | $kg{\cdot}m^{-3}$ | literature |
| solvent viscosity | $\eta_2$ | $8.9 \times 10^{-4}$ | $1.25 \times 10^{-3}$ | $kg{\cdot}m^{-1}{\cdot}s^{-1}$ | literature |
| solution density | $\rho_2$ | 999.2 | 1108 | $kg{\cdot}m^{-3}$ | measured |
| solution viscosity | $\eta_2$ | $(9.538 \pm 0.477) \times 10^{-4}$ | $(1.296 \pm 0.065) \times 10^{-3}$ | $kg{\cdot}m^{-1}{\cdot}s^{-1}$ | fit |
| layer density | $\rho_1$ | 1020 | 1127 | $kg{\cdot}m^{-3}$ | assumed |
| layer viscosity | $\eta_1$ | $(9.748 \pm 1.755) \times 10^{-4}$ | $(1.348 \pm 0.243) \times 10^{-3}$ | $kg{\cdot}m^{-1}{\cdot}s^{-1}$ | fit |
| layer shear modulus | $\mu_1$ | $(2.005 \pm 0.441) \times 10^4$ | $(2.016 \pm 0.444) \times 10^4$ | $kg{\cdot}m^{-1}{\cdot}s^{-2}$ | fit |
| loss tangent at 5 MHz | $\tan\delta$ | 1.515 | 2.081 | | calculated |
| layer thickness | $h_1$ | $(1.5 \pm 0.2) \times 10^{-9}$ | $(3.0 \pm 0.4) \times 10^{-9}$ | m | fit |
| adsorbed mass | $m$ | $153 \pm 28$ | $339 \pm 58$ | $ng{\cdot}cm^{-2}$ | calculated |

to the surface, resulting in a region of low solvent density very near the interface.[20,52] This serves to promote leucine adsorption by allowing it to place its nonpolar side chain in regions of low solvent density, where it will disrupt fewer solvent-solvent interactions than in the bulk, in accordance with the hydrophobic effect.[65] Therefore, the greater adsorption of leucine from $D_2O$ is reasonable based on its lower solubility compared to water.[66] This arises as a result of the greater strength of the bonding network in $D_2O$. Since the O-D–O bond is stronger than the corresponding hydrogen bond in water, rupturing of this bond in order to interact with the charged amine and carboxyl group in leucine is more difficult, which leads to decreased hydration.[67] Thus, since the energetic penalty of solvation by $D_2O$ is so high, leucine is more likely to reduce exposure of its nonpolar side chain, first by placing it in regions of lower solvent density near the surface, and eventually associating with the nonpolar polystyrene surface, in order to minimize its disruptive effect on the solvent bonding network. This phenomenon would be more pronounced in $D_2O$ than in $H_2O$. Moreover, the strength of the hydrophobic interaction would be greater in $D_2O$ than in $H_2O$, according to previous studies.[66] Another important factor when considering the adsorption of leucine to polystyrene is the differential orientation of water and $D_2O$ at the interface, as a result of quantum nuclear effects. Studies have shown that O–H bonds preferentially orient toward the air/water interface (a model hydrophobic surface) while O–D bonds orient toward the bulk.[68] In addition to solvation environment effects on leucine adsorption, these orientation differences between $H_2O$ and $D_2O$ at the interface likely play a significant role in its preferential adsorption from $D_2O$, where there are fewer dangling O–D bonds to interact with leucine's side chains, thereby enhancing its surface adsorption capability.[69] We further note that, since our solutions are not buffered, variations in pH may also contribute to differences in adsorbed amount.

## SFG

Fig. 4a shows the SFG spectra of 0.17 M leucine at the polystyrene–$D_2O$ interface (red points), and the control experiment in the absence of leucine (black points). A qualitative inspection of the data reveals that alkyl stretching modes are very prominent in the 2800–3000 $cm^{-1}$ region. One of the

unique features of nonlinear vibrational spectroscopy is that the response is coherent. As a result, the line shape is obtained by summing over the amplitude and phase of each oscillator/mode prior to squaring the result to obtain the spectral intensity (Eq. 5). A simple summation over Lorenztians may be used for the dominant modes when a homogeneous lineshape is assumed,

$$\chi^{(2)}_{\mathrm{Leu}} = \sum_{q=1}^{4} \frac{A_q}{\omega_{\mathrm{IR}} - \omega_q + i\Gamma_q}. \tag{7}$$

For each normal mode $q$ we consider $\omega_{\mathrm{IR}}$ is the incident IR frequency, $\omega_q$ is the normal mode frequency, $i = \sqrt{-1}$, $\Gamma_q$ is the homogeneous line width, and the numerator $A_q$ is the ensemble-averaged product of IR transition dipole moment and Raman transition polarizability. Values of these parameters obtained from a fit to the data (red line in Fig. 4a) are shown in Table 2.

**Table 2: Parameters used to fit the leucine in $D_2O$ on polystyrene data appearing in Fig. 4a to Eq. 7 ($q$ = 1–4) and water on polystyrene data from Fig. 4b to Eq. 8 ($q$ = 5 and 6).**

| $q$ | $\omega_q$ / cm$^{-1}$ | $A_q$ | $\Gamma_{h,q}$ / cm$^{-1}$ | $\Gamma_{i,q}$ / cm$^{-1}$ |
|---|---|---|---|---|
| 1 | 2852 | −2.7 | 5.5 | — |
| 2 | 2870 | −4.6 | 5.7 | — |
| 3 | 2900 | −4.4 | 15 | — |
| 4 | 2935 | −6.8 | 10 | — |
| 5 | 3200 | 0.2 | 5 | 95 |
| 6 | 3400 | 0.02 | 5 | 50 |

In the presence of water, the spectra look remarkably different. Fig. 4b shows the baseline polystryene–water response (black points) and in the presence of 0.17 M leucine (blue points). The overall reduction in intensity upon the addition of solute is typical for many osmolytes, attributed to a disruption of the interfacial hydrogen bonding network.[70,71] The leucine spectrum illustrates that, in addition to the broad response of the interfacial O–H stretching modes spanning nearly 1000 cm$^{-1}$, the alkyl modes are much less prevelant. The coherent nature of the SFG response doesn't necessarily 'bury' low amplitude modes in the presence of large background signals, as would occur in IR absorption or Raman scattering spectra. In SFG spectroscopy, such interference typically leads to amplification of the signal as a reult of the water-leucine cross term in $|\chi^{(2)}|^2$.

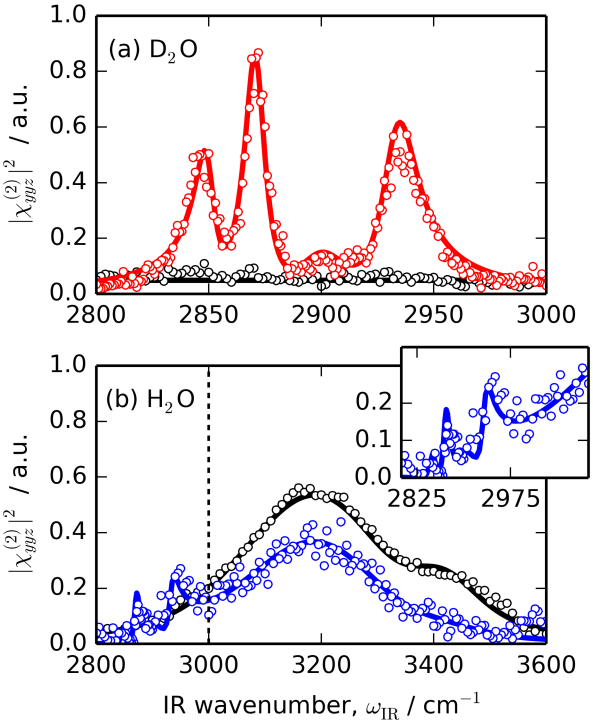


Figure 4: (a) SFG intensity spectrum of leucine in $D_2O$ adsorbed at the polystyrene surface (red points), fit to a model based on Eq. 7. The neat polystryene–$D_2O$ interface is shown in black. (b) SFG spectrum of leucine in $H_2O$ at the polystyrene surface (blue points), superimposed on the model created using Eq. 9 (blue line) The neat polystyrene–water interface is shown in black. The inset displays an enlarged portion of the 2800–3000 $cm^{-1}$ region.

The fact that the leucine modes appear weaker in water therefore points to the possibility that the adsorbed quantity and/or structure may be different from that in $D_2O$. We already know from the QCM-D data that there is roughly half the quantity of leucine on the surface in the case of water. We now use this information together with our SFG data to further interpret the spectra.

The inhomogeneous OH lineshape may be accounted for with a convolution of Lorenztian and Gaussian profiles,

$$\chi^{(2)}_{\text{water}} = \sum_{q=5}^{6} \int_0^{\infty} \frac{A_q}{\omega_{\text{IR}} - \omega_L + i\Gamma_{h,q}} \exp\left[\frac{(\omega_q - \omega_L)^2}{2\Gamma^2_{i,q}}\right] \mathrm{d}\omega_L \tag{8}$$

where $\Gamma_i$ is the inhomogeneous line width, and $\omega_L$ is the variable over which the integral is evaluated. In such cases, the homogeneous line widths $\Gamma_h$ are typically fixed at values determined from

vibrational dephasing lifetime experiments (here we have used $\Gamma_h = 5$ cm$^{-1}$). The broad features in the 3000–3500 cm$^{-1}$ region are due to the multitude of water O–H stretching environments. We have modelled this water response using two bands, centered at 3200 cm$^{-1}$ and 3400 cm$^{-1}$. The leucine C–H modes may be clearly observed in the 2800–3000 cm$^{-1}$ region, but their amplitudes are not significant enough to uniquely fit the peaks using a homogeneous model as was done in the case of $D_2O$. Such modest intensity is typical of C–H stretching modes of amino acids adsorbed onto polystyrene in water.[44] We therefore model the leucine/water response using

$$\chi^{(2)}_{\text{Leu-water}} = \chi^{(2)}_{\text{water}} + r \cdot \chi^{(2)}_{\text{Leu}} \tag{9}$$

where $r$ represents the fraction of the population of leucine on the surface in water compared to that in $D_2O$. This can be obtained from the adsorbed mass of leucine on polystyrene in water ($m_{\text{H}}$ in Table 1) and in $D_2O$ ($m_{\text{D}}$), resulting in $r = m_{\text{H}}/m_{\text{D}} = 0.45$. The spectrum predicted by Eq. 9 is indicated by the solid blue line in Fig. 4b. One can notice that the agreement with the measured spectra (points in Fig. 4b) is reasonable, including the apparent difference in the relative C–H mode strength as a result of their coherent superposition with the tailing of the hydrogen-bonded water O–H modes in the same region (enlarged in the inset to Fig. 4b). This indicates that the difference in intensity and overall appearance of the leucine $H_2O$ compared to $D_2O$ spectra may be attributed to a difference in the population of leucine on the polystyrene surface, with negligible difference in surface-adsorbed structure for the adsorbate between the two interfacial solvation environments.

## Implications for the role of solvent in biomolecular adsorption

Our finding that the structure of leucine adsorbed to polystyrene is similar, whether the solvent is $H_2O$ or $D_2O$, raises interesting questions on the role of solvent in the adsorption and structuring of biomolecules at surfaces. Although it is recognized that the solvent structure in the first 10–15 Å is highly dependent on the chemical and physical properties of the surface,[72,73] there is surprisingly little evidence of how this affects the molecules in their adsorbed state. A molecular dynamics

simulation of leucine in water adsorbed onto surfaces of varying hydrophobicity indicated that, as the hydrophobicity of the substrate increased, the surface water structure in the presence of adsorbed leucine has increasing similarity to that in the absence of leucine.[20] Studies of a diverse sampling of amino acid and peptide adsorption at both hydrophobic and hydrophilic surfaces illustrate that side chain composition, polarity, length, charge, and conformation heavily influence the extent of amino acid/peptide adsorption and surface structure.[31,32] In particular, it was found that the amphiphilic peptide LK$\alpha$14 (comprised of leucine and lysine residues) preferentially adsorbed to polystyrene via hydrophobic interactions through the dehydrated leucine side chains, while electrostatic interactions of the positively charged lysine side chain dictated adsorption behaviour to a hydrophilic silica surface.[32] Others studies report that adsorption of peptides can have a marked influence on interfacial water structure, as evidenced by changes in the signal intensity and ratio of the 3200 $cm^{-1}$ versus 3400 $cm^{-1}$ peaks in SFG spectra.[34] This highlights the role that solvent structure plays in the adsorption of biomolecules, and the close relationship between interfacial solvent structure and adsorbate structure. In addition to structural considerations, vibrational energy transfer and dissipation dynamics at the aqueous interface are known to be integral to adhesion processes.[74] It has been shown that interfacial energy transfer in $D_2O$ occurs through rapid and efficient transfer of vibrational energy through the O–D stretching mode, both along the surface and into the bulk, and that these interfacial dynamics are slower in $D_2O$ than in $H_2O$ but are unique to water.[75] The variability among amino acids, peptides, and proteins in terms of adsorption tendencies and strength, conformational changes upon adhesion, structure and orientation at the surface, and reversibility of adsorption require further investigation into the role of solvent in biomolecular adsorption at surfaces.

# Conclusions

Dissipation-monitoring quartz crystal microbalance and vibrational sum-frequency generation spectroscopy were used to study the adsorption of a hydrophobic amino acid onto a hydrophobic

surface in the presence of $H_2O$ and $D_2O$. Analysis of the QCM-D data using a Voigt model to account for the viscoelastic response of the damped surface environment resulted in the conclusion that more than twice as much leucine was adsorbed onto polystyrene when the solvent was $D_2O$. When the specific ratio of $H_2O$:$D_2O$ leucine surface mass was used in a model of the second-order nonlinear response, the intensity and overall appearance of the SFG spectral features was entirely accounted for. This is evidence for similar adsorbed structure in the two different solvent environments, highlighting the role of solvent in dictating the adsorbed quantity while not altering the interfacial structure at hydrophobic surfaces. This data supports the suitability of substituting $D_2O$ for $H_2O$ in spectroscopic studies of biological adsorption at hydrophobic surfaces. The extreme sensitivity of SFG towards molecular orientation, in conjunction with the mass sensitivity of QCM-D, make these techniques complementary for characterizing adsorption and structure at surfaces.

**Notes.** The authors declare no competing financial interest.

# Acknowledgement

This project was supported by a Discovery Grant from the Natural Science and Engineering Research Council of Canada (NSERC). The SFG spectrometer was purchased with assistance from the Canadian Foundation for Innovation Leader's Opportunity Fund, and the British Columbia Knowldege Development Fund. T.A.J. is grateful to NSERC for a PGS-M scholarship.

# References

(1) Moradi, S.; Hadjesfandiari, N.; Toosi, S. F.; Kizhakkedathu, J. N.; Hatzikiriakos, S. G. Effect of Extreme Wettability on Platelet Adhesion on Metallic Implants: From Superhydrophilicity to Superhydrophobicity. *Appl. Mater. Interfaces* **2016**, *8*, 17631–17641.

(2) Agarwal, R.; García, A. J. Biomaterial Strategies for Engineering Implants for Enhanced Osseointegration and Bone Repair. *Adv. Drug Delivery Rev.* **2015**, *94*, 53–62.

(3) Ye, S.; Wei, F.; Li, H.; Tian, K.; Luo, Y. Structure and Orientation of Interfacial Proteins Determined by Sum Frequency Generation Vibrational Spectroscopy: Method and Application. *Adv. Protein Chem. Struct. Biol.* **2013**, *93*, 213–255.

(4) Lu, J. R.; Zhao, X.; Yaseen, M. Protein Adsorption Studied by Neutron Reflection. *Curr. Opin. Coll. Inter. Sci.* **2007**, *12*, 9–16.

(5) Chena, H.; Yuana, L.; Song, W.; Wub, Z.; Lia, D. Biocompatible Polymer Materials: Role of Protein–Surface Interactions. *Prog. Poly. Sci.* **2008**, *33*, 1059–1087.

(6) Zhang, L.; Sun, Y. Molecular Simulation of Adsorption and its Implications to Protein Chromatography: A Review. *Biochem. Eng. J.* **2010**, *48*, 408–415.

(7) Krishnan, S.; Weinman, C. J.; Ober, C. K. Advances in Polymers For Anti-biofouling Surfaces. *J. Mater. Chem.* **2008**, *18*, 3405–3413.

(8) Elbert, D. L.; Hubbell, J. A. Surface Treatments of Polymers for Biocompatibility. *Annu. Rev. Mater. Sci.* **1996**, *26*, 365–394.

(9) Green, R. J.; Frazier, R. A.; Shakesheff, K. M.; Davies, M. C.; Roberts, C. J.; Tendler, S. J. Surface Plasmon Resonance Analysis of Dynamic Biological Interactions with Biomaterials. *Biomater.* **2000**, *21*, 1823–1835.

(10) Miyata, T.; Uragami, T.; Nakamae, K. Biomolecule-sensitive Hydrogels. *Adv. Drug Delivery Rev.* **2002**, *54*, 79–98.

(11) Adhikari, B.; Majumdar, S. Polymers in Sensor Applications. *Prog. Polym. Sci.* **2004**, *29*, 699–766.

(12) Jin, W.; Brennan, J. Properties and Applications of Proteins Encapsulated Within Sol-gel Derived Materials. *Anal. Chim. Acta* **2002**, *461*, 1–36.

(13) Pászti, Z.; Keszthelyi, T.; Hakkel, O.; Guczi, L. Adsorption of Amino Acids on Hydrophilic Surfaces. *J. Phys. Condens. Matter* **2008**, *20*, 224014.

(14) Watry, M. R.; Richmond, G. L. Orientation and Conformation of Amino Acids in Monolayers Adsorbed at an Oil/water Interface as Determined by Vibrational Sum-Frequency Spectroscopy. *J. Phys. Chem. B* **2002**, *106*, 12517–12523.

(15) Ji, N.; Shen, Y.-R. Optically Active Sum Frequency Generation From Molecules With a Chiral Center: Amino Acids as Model Systems. *J. Am. Chem. Soc.* **2004**, *126*, 15008–15009.

(16) Du, Q.; Freysz, E.; Shen, Y. R. Vibrational Spectra of Water Molecules at Quartz/Water Interfaces. *Phys. Rev. Lett.* **1994**, *72*, 238–241.

(17) Ong, S.; Zhao, X.; Eisenthal, K. B. Polarization of Water Molecules at a Charged Interface: Second Harmonic Studies of the Silica/Water Interface. *Chem. Phys. Lett.* **1992**, *191*, 327–335.

(18) Jena, K. C.; Hore, D. K. Variation of Ionic Strength Reveals the Interfacial Water Structure at a Charged Mineral Surface. *J. Phys. Chem. C* **2009**, *113*, 15364–15372.

(19) Hall, S. A.; Hickey, A. D.; Hore, D. K. Structure of Phenylalanine Adsorbed on Polystyrene From Nonlinear Vibrational Spectroscopy Measurements and Electronic Structure Calculations. *J. Phys. Chem. C* **2010**, *114*, 9748–9757.

(20) Trudeau, T. G.; Hore, D. K. Hydrophobic Amino Acid Adsorption on Surfaces of Varying Wettability. *Langmuir* **2010**, *26*, 11095–11102.

(21) Hall, S. A.; Jena, K. C.; Trudeau, T. G.; Hore, D. K. Structure of Leucine Adsorbed on Polystyrene from Nonlinear Vibrational Spectroscopy Measurements, Molecular Dynamics Simulations, and Electronic Structure Calculations. *J. Phys. Chem. C* **2011**, *115*, 11216–11225.

(22) Hall, S. A.; Jena, K. C.; Covert, P. A.; Roy, S.; Trudeau, T. G.; Hore, D. K. Molecular-Level

Surface Structure from Nonlinear Vibrational Spectroscopy Combined with Simulations. *J. Phys. Chem. B* **2014**, *118*, 5617–5636.

(23) Dixon, M. C. Quartz Crystal Microbalance with Dissipation Monitoring: Enabling Real-Time Characterization of Biological Materials and Their Interactions. *J. Biomol. Techn.* **2008**, *19*, 151–158.

(24) Voinova, M. V.; Rodahl, M.; Jonson, M.; Kasemo, B. Viscoelastic Acoustic Response of Layered Polymer Films at Fluid–Solid Interfaces: Continuum Mechanics Approach. *Physica Scripta* **1999**, *59*, 391–396.

(25) Berglin, M.; Pinori, E.; Sellborn, A.; Andersson, M.; Hulander, M.; Elwing, H. Fibrinogen Adsorption and Conformational Change on Model Polymers: Novel Aspects of Mutual Molecular Rearrangement. *Langmuir* **2009**, *25*, 5602–5608.

(26) Gormally, M.; McKibben, R.; Johal, M.; Selassie, C. Controlling Tyrosinase Activity on Charged Polyelectrolyte Surfaces: A QCM-D Analysis. *Langmuir* **2009**, *25*, 10014–10019.

(27) Höök, F.; Voros, J.; Rodahl, M.; Kurrat, R.; Boni, P.; Ramsden, J. J.; Textor, M.; Spencer, N. D.; Tengvall, P.; Gold, J. et al. A Comparative Study of Protein Adsorption on Titanium Oxide Surfaces Using In situ Ellipsometry, Optical Wavefuide Lightmode Spectroscopy, and Quartz Crystal Microbalance/Dissipation. *Coll. Surf. B* **2002**, *24*, 155–170.

(28) Stålgren, J. J. R.; Eriksson, J.; Boschkova, K. A Comparative Study of Surfactant Adsorption on Model Surfaces Using the Quartz Crystal Microbalance and the Ellipsometer. *J. Colloid Interface Sci.* **2002**, *253*, 190–195.

(29) Bieri, M.; Burgi, T. Adsorption Kinetics, Orientation, and Self-Assembling of *N*-Acetyl-*l*-cysteing on Gold: A Combined ATR-IR, PM-IRRAS, and QCM Study. *J. Phys. Chem. B.* **2005**, *109*, 22476–22485.

(30) Bieri, M.; Bürgi, T. Adsorption Kinetics of L-Glutathione on Gold and Structural Changes During Self-assembly: An In situ ATR-IR and QCM Study. *Phys. Chem. Chem. Phys.* **2006**, *8*, 513–520.

(31) Onorato, R. M.; Yoon, A. P.; Lin, J. T.; Somorjai, G. A. Adsorption of Amino Acids and Dipeptides to the Hydrophobic Polystyrene Interface Studied by SFG and QCM: The Special Case of Phenylalanine. *J. Phys. Chem. C* **2012**, *116*, 9947–9954.

(32) Mermut, O.; Phillips, D. C.; York, R. L.; McCrea, K. R.; Ward, R. S.; Somorjai, G. A. In Situ Adsorption Studies of a 14-Amino Acid Leucine-Lysine Peptide onto Hydrophobic Polystyrene and Hydrophilic Silica Surfaces Using Quartz Crystal Microbalance, Atomic Force Microscopy, and Sum Frequency Generation Vibrational Spectroscopy. *J. Am. Chem. Soc.* **2006**, *128*, 3598–3607.

(33) Phillips, D. C.; York, R. L.; Mermut, O.; McCrea, K. R.; Ward, R. S.; Somorjai, G. A. Side Chain, Chain Length, and Sequence Effects on Amphiphilic Peptide Adsorption at Hydrophobic and Hydrophilic Surfaces Studied by Sum-Frequency Generation Vibrational Spectroscopy and Quartz Crystal Microbalance. *J. Phys. Chem. C* **2007**, *111*, 255–261.

(34) York, R. L.; Holinga, G. J.; Somorjai, G. A. An Investigation of the Influence of Chain Length on the Interfacial Ordering of L-Lysine and L-Proline and their Homopeptides at Hydrophobic and Hydrophilic Interfaces Studied by Sum Frequency Generation and Quartz Crystal Microbalance. *Langmuir* **2009**, *25*, 9369–9374.

(35) Liu, C.; Thormann, E.; Claesson, P. M.; Tyrode, E. Surface Grafted Chitosan Gels. Part 1. Molecular Insight into the Formation of Chitosan and Poly(acrylic acid) Multilayers. *Langmuir* **2014**, *30*, 8866–8877.

(36) Shen, S.-Y.; Schlag, E. W.; Selzle, H. L.; Yang, D.-Y. Molecular Dynamics of Hydrogen Bonds in Protein–$D_2O$: The Solvent Isotope Effect. *J. Phys. Chem. A* **2008**, *112*, 797–802.

(37) Kong, J.; Yu, S. Fourier Transform Infrared Spectroscopic Analysis of Protein Secondary Structure. *Acta Biochim. Biophys. Sinica* **2007**, *39*, 549–559.

(38) Efimova, Y. M.; Haemers, S.; Wierczinski, B.; Norde, W.; van Well, A. A. Stability of Globular Proteins in H2O and D2O. *Biopolymers* **2006**, *85*, 264–273.

(39) Makhatadze, G. I.; Clore, G. M.; Gronenborn, A. M. Solvent Isotope Effect and Protein Stability. *Nat. Struct. Biol.* **1995**, *2*, 852–855.

(40) Huyghues-Despointes, B.; Scholtz, M.; Pace, N. Protein Conformational Stabilities can be determined from Hydrogen Exchange Rates. *Nat. Struct. Biol.* **1999**, *6*, 910–912.

(41) Trudeau, T. G.; Jena, K. C.; Hore, D. K. Water Structure at Solid Surfaces of Varying Hydrophobicity. *J. Phys. Chem. C* **2009**, *113*, 20002–20008.

(42) Scatena, L. F.; Brown, M. G.; Richmond, G. L. Water at Hydrophobic Surfaces: Weak Hydrogen Bonding and Strong Orientation Effects. *Science* **2001**, *292*, 908–912.

(43) Alaeddine, S.; Nygren, H. The Adsorption of Water and Amino Acids on to Hydrophilic and Hydrophobic Quartz Surfaces. *Coll. Surf. B* **1995**, *6*, 71–79.

(44) Holinga, G. J.; York, R. L.; Onorato, R. M.; Thompson, C. M.; Webb, N. E.; Yoon, A. P.; Somorjai, G. A. An SFG Study of Interfacial Amino Acids at the Hydrophilic $SiO_2$ and Hydrophobic Deuterated Polystyrene Surfaces. *J. Am. Chem. Soc.* **2011**, *133*, 6243–6253.

(45) Weidner, T.; Samuel, N. T.; McCrea, K.; Gamble, L. J.; Ward, R. S.; Castner, D. G. Assembly and Structure of $\alpha$-helical Peptide Films on Hydrophobic Fluorocarbon Surfaces. *Biointerphases* **2010**, *5*, 9–16.

(46) Weidner, T.; Apte, J. S.; Gamble, L. J.; Castner, D. G. Probing the Orientation and Conformation of $\alpha$-Helix and $\beta$-Strand Model Peptides on Self-Assembled Monolayers Using Sum Frequency Generation and NEXAFS Spectroscopy. *Langmuir* **2009**, *26*, 3433–3440.

(47) Weidner, T.; Breen, N. F.; Li, K.; Drobny, G. P.; Castner, D. G. Sum Frequency Generation and Solid-State NMR Study of the Structure, Orientation, and Dynamics of Polystyrene-Adsorbed Peptide. *Proc. Natl. Acad. Sci. U.S.A.* **2010**, *107*, 13288–13293.

(48) Fu, L.; Xiao, D. Q.; Wang, Z.; Batista, V. S.; Yan, E. C. Y. Chiral Sum Frequency Generation for In Situ Probing Proton Exchange in Antiparallel $\beta$-Sheets at Interfaces. *J. Am. Chem. Soc.* **2013**, *135*, 3592–3598.

(49) Roy, S.; Naka, T. L.; Hore, D. K. Enhanced Understanding of Amphipathic Peptide Adsorbed Structure by Modeling of the Nonlinear Vibrational Response. *J. Phys. Chem. C* **2013**, *117*, 24955–24966.

(50) Collier, G.; Vellore, N. A.; Yancey, J. A.; Stuart, S. J.; Latour, R. A. Comparison Between Empirical Protein Force Fields for the Simulation of the Adsorption Behavior of Structured LK Peptides on Functionalized Surfaces. *Biointerphases* **2012**, *7*, 1–19.

(51) Deighan, M.; Pfaendtner, J. Exhaustively Sampling Peptide Adsorption with Metadynamics. *Langmuir* **2013**, *29*, 7999–8009.

(52) Krause, K. D.; Roy, S.; Hore, D. K. Interplay Between Adsorbed Peptide Structure, Trapped Water, and Surface Hydrophobicity. *Biointerphases* **2017**, *12*, 02D407.

(53) Reviakine, I.; Johannsmann, D.; Richter, R. P. Hearing What You Cannot See and Visualizing What You Hear: Interpreting Quartz Crystal Microbalance Data from Solvated Interfaces. *Anal. Chem.* **2011**, *83*, 8838–8848.

(54) Dunér, G.; Thormann, E.; Dèdinaitò, A. Quartz Crystal Microbalance with Dissipation (QCM-D) studies of the viscoelastic response from a continuously growing grafted polyelectrolyte layer. *J. Coll. Inter. Sci.* **2013**, *408*, 229–239.

(55) Liu, S.; Kim, J. Application of Kevin-Voigt Model in Quantifying Whey Protein Adsorption on Polyethersulfone Using QCM-D. *J. Assoc. Lab. Autom.* **2009**, *Aug*, 213–220.

(56) Sultanova, N.; Kasarova, S.; Kokolov, I. Dispersion Properties of Optical Polymers. *Acta Phys. Polonica A* **2009**, *116*, 585–587.

(57) Malitson, I. H. A Redetermination of Some Optical Properties of Calcium Fluoride. *Appl. Opt.* **1963**, *2*, 1103–1107.

(58) Segelstein, D. J. The Complex Refractive Index of Water. M.Sc. thesis, University of Missouri, Kansas City, 1981.

(59) Max, J.-J.; Chapados, C. Isotope Effects in Liquid Water by Infrared Spectroscopy. III. $H_2O$ and $D_2O$ Spectra from 6000–0 $cm^{-1}$. *J. Chem. Phys.* **2009**, *131*, 184505.

(60) Harp, G. P.; Gautam, K. S.; Dhinojwala, A. Probing Polymer/Polymer Interfaces. *J. Am. Chem. Soc.* **2002**, *124*, 7908–7909.

(61) Harp, G. P.; Rangwalla, H.; Yeganeh, M. S.; Dhinojwala, A. Infrared-Visible Sum Frequency Generation Spectroscopic Study of Molecular Orientation at Polystyrene/Comb-Polymer Interfaces. *J. Am. Chem. Soc.* **2003**, *125*, 11283–11290.

(62) Nash, S. G. A Survey of Truncated-Newton Methods. *J. Comput. Appl. Math.* **2000**, *124*, 45–49.

(63) Höök, F.; Kasemo, B.; Nylander, T.; Fant, C. Variations in Coupled Water, Viscoelastic Properties, and Film Thickness of a Mefp-1 Protein Film during Adsorpt ion and Cross-Linking: A Quartz Crystal Microbalance with Dissipation Monitoring, Ellipsometry, and Surface Plasmon Resonance Study. *Anal. Chem.* **2001**, *73*, 5796–5804.

(64) Tagaya, M.; Ikoma, T.; Hanagata, N.; Yoshioka, T.; Tanaka, J. Competitive Adsorption of Fibronectin and Albumin on Hydroxyapatite Nanocrystals. *Sci. Technol. Adv. Mater.* **2011**, *12*, 034411.

(65) Southall, N. T.; Dill, K. A.; Haymet, A. D. J. A View of the Hydrophobic Effect. *J. Phys. Chem. B* **2002**, *106*, 521–533.

(66) Kresheck, G. C.; Schneider, H.; Scheraga, H. A. The Effect of $D_2O$ on the Thermal Stability of Proteins. Thermodynamic Parameters for the Transfer of Model Compounds from $H_2O$ to $D_2O$. *J. Phys. Chem.* **1965**, *69*, 3132–3144.

(67) Broutin, I.; Riès-Kautt, M.; Ducruix, A. Lysozyme Solubility in $H_2O$ and $D_2O$ Solutions as a Function of Sodium Chloride Concentration. *J. Appl. Cryst.* **1995**, *28*, 614–617.

(68) Nagata, Y.; Pool, R. E.; Backus, E. H. G.; Bonn, M. Nuclear Quantum Effects Affect Bond Orientation of Water at the Water-Vapor Interface. *Phys. Rev. Lett.* **2012**, *109*, 226101.

(69) Liu, J.; Andino, R. S.; Miller, C. M.; Chen, X.; Wilkens, D. M.; Ceriotti, M.; Manolopoulos, D. E. A Surface-Specific Isotope Effect in Mixtures of Light and Heavy Water. *J. Phys. Chem. C* **2013**, *117*, 2944–2951.

(70) Chen, X.; Yang, T.; Kataoka, S.; Cremer, P. S. Specific Ion Effects on Interfacial Water Structure Near Macromolecules. *J. Am. Chem. Soc.* **2007**, *129*, 12272–12279.

(71) Zhang, Y.; Cremer, P. S. Chemistry of Hofmeister Anions and Osmolytes. *Ann. Rev. Phys. Chem.* **2010**, *61*, 63–83.

(72) Jena, K. C.; Hore, D. K. Water Structure at Solid Surfaces and its Implications for Biomolecule Adsorption. *Phys. Chem. Chem. Phys.* **2010**, *12*, 14383–14404.

(73) Stiopkin, I. V.; Weeraman, C.; Pieniazek, P. A.; Shalhout, F. Y.; Skinner, J. L.; Benderskii, A. V. Hydrogen Bonding at the Water Surface Revealed by Isotopic Dilution Spectroscopy. *Nature* **2011**, *474*, 192–195.

(74) Zhang, Z.; Piatkowski, L.; Bakker, H. J.; Bonn, M. Interfacial Water Structure Revealed by Ultrast Two-dimensional Surface Vibrational Spectroscopy. *J. Chem. Phys.* **2011**, *135*, 021101.

(75) Zhang, Z.; Piatkowski, L.; Bakker, H. J.; Bonn, M. Ultrafast Vibrational Energy Transfer at

the Water/Air Interface Revealed by Two-dimensional Surface Vibrational Spectroscopy. *Nat. Chem.* **2011**, *3*, 888–893.

# Graphical TOC Entry